Structural, thermal, and electronic properties of $Fe_2VSi_{1-x}Al_x$

C. S. Lue,[1] Y.-K Kuo,[2,*] S.-N. Horng,[1] S. Y. Peng,[2] and C. Cheng[1]
[1]*Department of Physics, National Cheng Kung University, Tainan 70101, Taiwan*
[2]*Department of Physics, National Dong Hwa University, Hualien 97401, Taiwan*
(Received 6 September 2004; revised manuscript received 9 December 2004; published 23 February 2005)

In order to access the influence of the local environment on the structural and electronic properties of Fe_2VSi, we investigated the $Fe_2VSi_{1-x}Al_x$ series of compounds by measuring electrical resistivity (ρ), thermal conductivity (κ), Seebeck coefficient (S), as well as heat capacity (C_p) as a function of temperature. For Fe_2VSi, all obtained quantities exhibit anomalous features near the structural transition temperature $T_s \approx 123$ K. For the nonstoichiometric compounds $Fe_2VSi_{1-x}Al_x$, these anomalies remain evident but appear to be weaker as increasing Al concentration. The corresponding transition temperature T_s decreases with x, indicating the suppression of the low-temperature tetragonal phase via Al doping in Fe_2VSi. Theoretical studies with *ab initio* calculations were also employed to investigate the present structural and magnetic phase transition. Both theoretical results and experimental observations consistently yield a possible disappearance of the structural transition beyond a critical concentration $x_C \approx 0.25$. In addition, several aspects regarding the structural and electronic properties were compared to those of other Heusler alloys.

DOI: 10.1103/PhysRevB.71.064202 PACS number(s): 72.15.Eb, 71.20.Lp, 81.30.−t

I. INTRODUCTION

Cubic $L2_1$ Heusler alloys (Cu_2MnAl type) with general formula X_2YZ, where X and Y are transition metals and Z often is an element with *sp*-type valence electrons from columns III through VI in the periodic table, have been of considerable interest due to their unusual transport and magnetic properties. Semiconductors, semimetals, normal Pauli metals, weak ferromagnets, as well as half-metallic ferromagnets have been found to exist in this class of materials.[1–4] The variety of physical behavior observed in these Heusler compounds seems to be related to strong modifications of the electronic structure near the Fermi level.[5–8]

In the view of the structural stabilization, the cubic $L2_1$ phase for the materials of this family is usually more preferable at low temperatures as competed with other phases. As a result, the occurrence of structural transformation at low temperatures is not commonly seen in these Heusler-type alloys. Ni_2MnGa, Co_2NbSn, Co_2NiGa, and Ni_2FeGa are a few prototype examples which exhibit a first-order transition from a high-temperature cubic structure to a low-temperature tetragonal or orthorhombic structure.[9–12] Such a transition occurring in the ferromagnetic state is particularly appealing, due to the possibility to observe a magnetic-field-induced shape memory effect.[13–16] Therefore, finding and investigating a system with coupled magnetostructural transition is of great importance for both fundamental research and technological application.[17–22]

Fe_2VSi, which also belongs to the group of Heusler compounds, exhibits a structural transition along with antiferromagnetic (AFM) ordering at $T_s = 123$ K.[23–25] Although the AFM character cannot be obtained from the bulk susceptibility measurements,[26] mainly attributed to the antisite disorder effect, the neutron scattering data did reveal a complex AFM state at low temperatures.[27] Also the anomalous feature near the structural transition of Fe_2VSi has been found to be very sample dependent. For example, no anomalies have been observed in the previously reported resistivity and Seebeck coefficient data.[28,29] Hence, several aspects are still not well established for Fe_2VSi.

In this study, we have carried out measurements of electrical resistivity (ρ), thermal conductivity (κ), Seebeck coefficient (S), as well as heat capacity (C_p) on the $Fe_2VSi_{1-x}Al_x$ series of alloys. Altering the composition allows a change of these characteristics, and results are valuable for understanding the influence of the local environment on the structural and electronic properties of Fe_2VSi. It is found that the partial substitution of Si with Al leads to a decrease in the transition temperature (T_s) and consequently a disappearance of the structural transition beyond a critical composition $x_c \approx 0.25$. In a parallel study, *ab initio* calculations were also employed to investigate the phase transition features of $Fe_2VSi_{1-x}Al_x$. Theoretical results were found to be in good agreement with experimental observations.

II. EXPERIMENTAL DETAILS

Polycrystalline $Fe_2VSi_{1-x}Al_x$ alloys with $x = 0$, 0.02, 0.05, 0.09, 0.12, 0.15, 0.20, and 0.25 were prepared by an ordinary arc-melting technique. Briefly, a mixture of appropriate amounts of high-purity elemental metals was placed in a water-cooled copper crucible and then melted several times in an argon flow arc melter. The weight loss during melting is less than 0.5% for each compound. To promote homogeneity, these ingots were annealed in a vacuum-sealed quartz tube at 800 °C for two days, and followed by furnace cooling. This is a typical process to form in a single-phase $L2_1$ (Heusler-type) structure.[30]

Electrical resistivity for the $Fe_2VSi_{1-x}Al_x$ alloys were obtained by a standard dc four-terminal method. Most materials were measured in a close-cycle refrigerator, while some samples were carried out in a liquid helium cryostat down to 2 K. Thermal conductivity measurement was performed in a close-cycle refrigerator over temperatures from

8 to 300 K, using a direct heat-pulse technique. Samples were cut to a rectangular parallelepiped shape of typical size of $1.5\times1.5\times5.0$ mm^3 with one end glued (with thermal epoxy) to a copper block that served as a heat sink, while a calibrated chip resistor as a heat source was glued to the other end. The temperature difference was measured by using an *E*-type differential thermocouple with junctions thermally attached to two well-separated positions along the longest axis of the sample. The temperature gradient was controlled to be less than 1 K to minimize the heat loss through radiation. During measurements the sample space is maintained in a good vacuum (better than 10^{-4} Torr).

For the thermoelectric power measurements, Seebeck voltages were detected using a pair of thin Cu wire electrically connected to the sample with sliver paint at the same positions as the junctions of differential thermocouple. The stray thermal emfs are eliminated by applying long current pulses ($\sim$100 s) to the chip resistor, where the pulses appear in an off-on-off sequence. All experiments were performed during warming with a rate slower than 20 K/h. The reproducibility of κ and S measurements is better than 2%, while the absolute accuracy of κ is approximately 20%, which mainly arises from the error in the determination of sample dimensions.

Relative specific heats were performed with a high resolution ac calorimeter, using chopped light as a heat source. The absolute values of the molar heat capacity for $Fe_2VSi_{1-x}Al_x$ were obtained by normalizing the ac data to the isostructural compound Co_2NbSn at 300 K.[31] Here we assume that the Heusler alloys with the same chemical formula and crystal structure should possess a comparable molar heat capacity at high temperatures. Photoabsorbing PbS film were evaporated on samples, which were sanded to a thickness of about 0.2 mm to ensure "one-dimensional" heat flow. The averaged and oscillating temperatures (T_{ac}) of the sample were detected by an *E*-type thermocouple, attached with small amount of GE varnish. The frequency dependence of T_{ac} was measured at various temperatures to determine the correct range of chopping frequencies. For appropriately chosen chopping frequency (typically 2–12 Hz), the magnitude of the temperature oscillation is inversely proportional to the total heat capacity (including sample and addendum). Several specimens were examined to check reproducibility. More details of the measurement techniques can be found elsewhere.[32]

III. RESULTS AND DISCUSSION

A. X-ray diffraction

A room-temperature x-ray diffraction taken with Cu K_α radiation on powder $Fe_2VSi_{1-x}Al_x$ samples is shown in Fig. 1(a). It is seen that the diffraction spectra in these alloys were identified as the expected $L2_1$ structure, with no sign of the presence of other phases. A more detailed analysis of the x-ray data, in which the Heusler-type structure was refined with the Rietveld method. We thus obtained the lattice constant, a, for each composition. The variation of lattice constant as a function of x is illustrated in Fig. 1(b). It clearly demonstrates that the value of lattice constant increases as

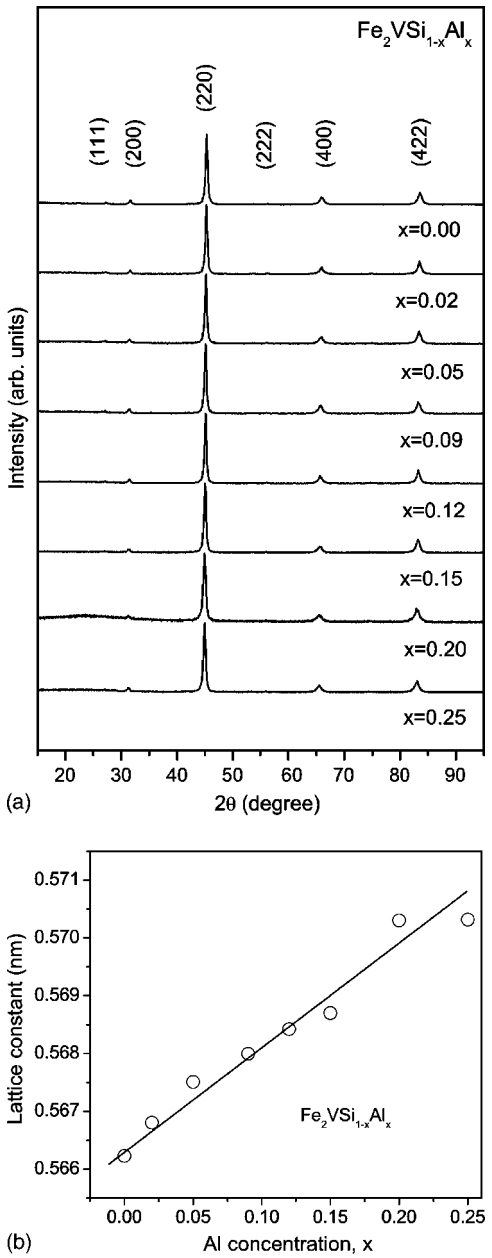

FIG. 1. (a) X-ray diffraction patterns in $Fe_2VSi_{1-x}Al_x$. (b) Lattice parameter as a function of Al concentration x. The solid line is guided to the eye for the tendency.

Fe_2VSi deviates from its stoichiometry, indicating that the Si sites are successfully replaced by Al atoms, according to the Vigard's law.

B. Electrical resistivity

The T-dependent electrical resistivity of Fe_2VSi is plotted in Fig. 2(a). The electrical transport at high temperatures exhibits quasilinear behavior, a typical temperature variation for ordinary metals. With decreasing temperature, a steep fall in ρ is found near $T_s=123$ K, close to the reported result.[23] Also the entire $\rho(T)$ feature shows no visible change under an external magnetic field of 5 T, as expected for the anti-

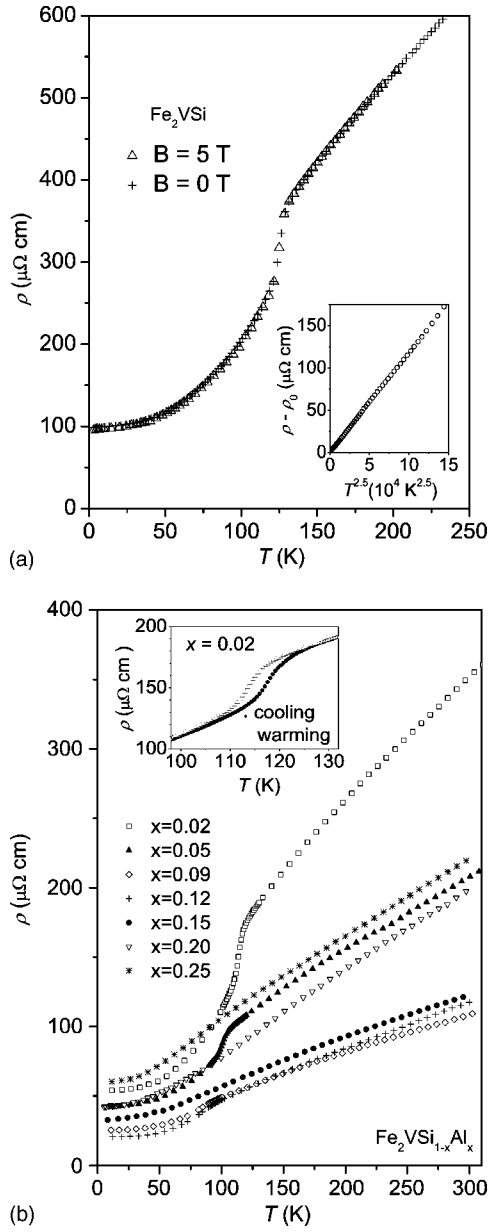

FIG. 2. (a) Temperature dependences of the electrical resistivity of Fe_2VSi measured on heating in zero magnetic field and 5 T. Inset: a linear low-temperature character of $\rho(T)$-ρ_0 in the AFM state from 2 to 120 K in $T^{2.5}$ coordinates. (b) Evolution of the temperature-dependent electrical resistivity in $Fe_2VSi_{1-x}Al_x$. The inset represents the thermal hysteresis behavior in the vicinity of T_s for $Fe_2VSi_{0.98}Al_{0.02}$.

ferromagnetic nature for this material. The residual resistivity $\rho_0 = 98\ \mu\Omega$ cm is a bit larger than that reported by Endo *et al.* ($\rho_0 \approx 35\ \mu\Omega$ cm),[23] reflecting the presence of crystallographic disorder, mainly from antisite between Fe and V atoms, in our Fe_2VSi sample. Regardless, the determined transition temperature is still identical with other published values,[23,34] indicating little effect on the transition temperature from disorder in Fe_2VSi.

Below T_s, $\rho(T)$ is fit well in a fairly wide temperature region to the relation

TABLE I. Phase transition temperature determined from the minimum of dS/dT, transition width determined from the width of dS/dT, exponent deduced from the low-T resistivity, and entropy change associated with the transition for $Fe_2VSi_{1-x}Al_x$.

x	T_s (K)	ΔT (K)	n	ΔS (R)
0.00	123	4	2.5	0.236
0.02	117	3	2.9	0.166
0.05	112	9	2.7	0.156
0.09	88	10	2.8	0.096
0.12	87	13	3.5	0.059
0.15	62	15	2.0	
0.20	46	22	1.9	

$$\rho(T) = \rho_0 + AT^n, \tag{1}$$

with $n \simeq 2.5$, as drawn in the inset of Fig. 2(a). It is worthwhile mentioning that the deviation from a T^2 law in $\rho(T)$ in the AFM state suggests unusual magnetism for this material, such as a half-metallic antiferromagnet proposed by Endo *et al.*[23] However, the band structure calculations indicate no such a possibility for this compound in the AFM state.[33] The low-T resistivity of antiferromagnetic Pd_2MnIn also shows a tendency towards a $T^{2.4}$ dependence,[35] close to the present case of Fe_2VSi. In fact, such a power law fit on the low-temperature resistivity yields different exponents for the non-stoichiometric $Fe_2VSi_{1-x}Al_x$ alloys (see Table I). In these regards, $\rho(T)$ at low temperatures may represent a combination of electron-electron, electron-phonon, electron-magnon scattering, all of which are expected to be significant but different weight for different composition.

Upon Al substitution for Si, the magnitude of electrical resistivity tends to reduce with increasing x in the low Al content samples ($x \leqslant 0.12$). The marked drop in ρ corresponding to the occurrence of structural phase transition is also seen in these $Fe_2VSi_{1-x}Al_x$ alloys, as demonstrated in Fig. 2(b). The anomalous feature becomes weaker and the transition temperature T_s shifts to lower temperatures as increasing Al concentration. In the inset of Fig. 2(b), a well-defined thermal hysteresis loop of about 4 K around T_s is given for $Fe_2VSi_{0.98}Al_{0.02}$, indicative of a first-order character for the presented phase transition. On the other hand, the overall resistivity gradually increases with a further addition of Al greater than $x = 0.12$. This observation is presumably attributed to the disorder effect which appears in all compositions. Such a disorder has a minor influence on the electrical transport as well as structural transition for the low Al-substituted samples, but greatly affects those properties with increasing Al content. As a consequence, an increase of residual resistivity together with a significant suppression of the anomalous features at phase transitions are observed in the resistivity data for $x > 0.12$.

C. Thermal conductivity

The T-dependent thermal conductivity for the stoichiometric Fe_2VSi is displayed in Fig. 3(a). A broad maximum

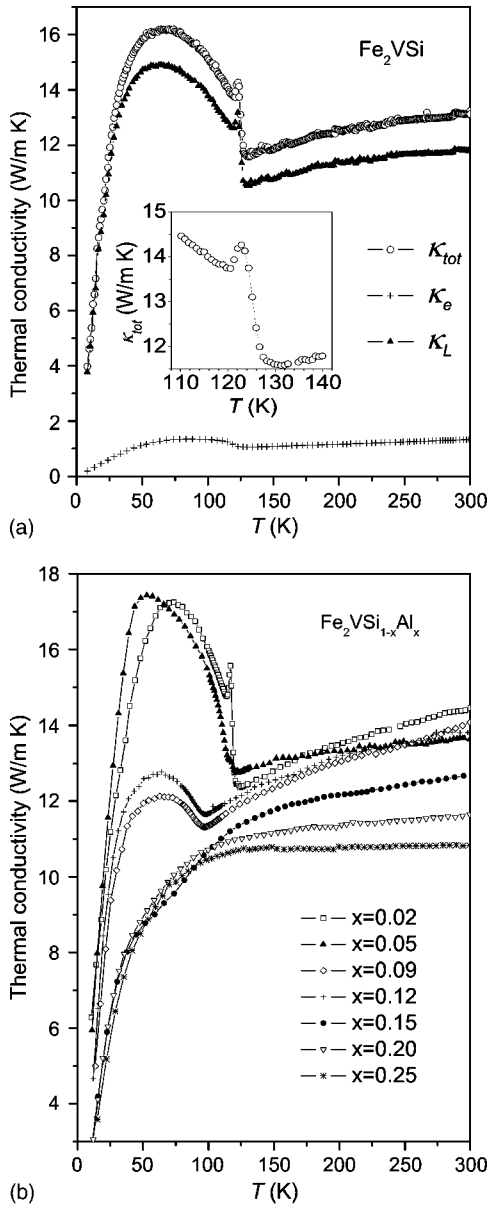

FIG. 3. (a) Thermal conductivity as function of temperature for Fe_2VSi. Estimated electronic (κ_e) and lattice (κ_L) contributions to the total thermal conductivity are given. Inset: a blow-up plot for the observed thermal conductivity near the transition. (b) Evolution of the temperature-dependent thermal conductivity in $Fe_2VSi_{1-x}Al_x$.

appears at around 60 K which is due to the reduction of thermal scattering at low temperatures. The maximum takes place at the temperature where the phonon mean free path is approximately equal to the crystal site distance. Around T_s, κ exhibits a steplike drop accompanied by a spiky jump [see the inset of Fig. 3(a)]. In general, the total thermal conductivity for a metal can be expressed as a sum of lattice (κ_L) and electronic (κ_e) terms: $\kappa=\kappa_L+\kappa_e$. The electronic contribution is estimated by means of the Wiedemann-Franz law: $\kappa_e\rho/T=L_0$. Here ρ is the dc electrical resistivity and $L_0=2.45\times10^{-8}$ W Ω K^{-2} is the Lorentz number. We thus calculated κ_e using the Wiedemann-Franz law and measured ρ data. The lattice thermal conductivity is taken as the difference between κ and κ_e. It is apparent that the abrupt fall in the vicinity of the transition is not due to the electronic contribution, but is essentially caused by the reduction of lattice thermal conductivity.

Another peculiar feature in κ is the presence of a spiky jump near T_s, which is also associated with additional lattice effects. It should be pointed out that similar κ behavior have been found in the isostructural Ni_2MnGa system near its structural transition.[36] Although the origin of this anomaly is not yet understood at this moment, heat carried by soft phonons during the phase transition may be responsible for this observation.[37]

For the nonstoichiometric compounds $Fe_2VSi_{1-x}Al_x$ with low substitution level ($x\leqslant0.12$), the anomalous feature in κ near T_s remains evident, as shown in Fig. 3(b). The value of room-temperature thermal conductivity for compositions with $x\leqslant0.12$ is found to be nearly equal with a magnitude of approximately 13–14 (W/K m), and the small variation of κ(300 K) in these alloys is within the uncertainty of our measurement technique. The jump in κ is still visible for the slightly substituted alloy $Fe_2VSi_{0.98}Al_{0.02}$, but smears out for the samples with $x\geqslant0.05$. This phenomenon is presumably due to the anisotropic effect for the heat transport, or defects which may wipe out the critical cusp in κ. Upon further replacing Si with Al ($x>0.12$), a dramatic change in the T-dependent thermal conductivity is seen as the low-temperature broad maximum disappears. Such an observation suggests a significant enhancement of point defects scattering with phonons[38] in these highly Al-substituted samples, being consistent with the electrical resistivity data.

D. Seebeck coefficient

Figure 4(a) illustrates the temperature-dependent Seebeck coefficient for Fe_2VSi. The values of Seebeck coefficient are negative in the temperature range we investigated, signifying that Fe_2VSi is an n-type material. The structural transition of Fe_2VSi manifests itself by the abrupt drop in S. It is known that the Seebeck coefficient measurement is a sensitive probe of energy relative to the Fermi surface and the results would reveal information about the Fermi level band structure. Since S varies rather linearly with T at high temperatures, indicating that diffusion Seebeck coefficient dominates the observed S in the high-T phase. Hence, one can extract the value of E_F through the classical formula $|S|=\pi^2k_B^2T/2eE_F$, assuming a one-band model with an energy-independent relaxation time. The value of $E_F\sim1.57$ eV was thus obtained by fitting the data between 140 and 300 K, in good agreement with the metallic nature for Fe_2VSi. Note that this value represents a measure from the bottom of conduction band to the Fermi level. With this fit, it yielded a nonzero S by extrapolating the linear behavior to $T\rightarrow0$, indicative of the departure from the free-electron scenario.[39,40]

With Al substitution for Si, the sign of S remains negative for all studied compositions, as shown in Fig. 4(b). The slope of S above T_s is almost independent of the substitution level in these alloys, indicating little or no E_F shift in the paramagnetic state via Al doping. The anomalies in the vicinity of transitions are still apparent for the low Al content samples,

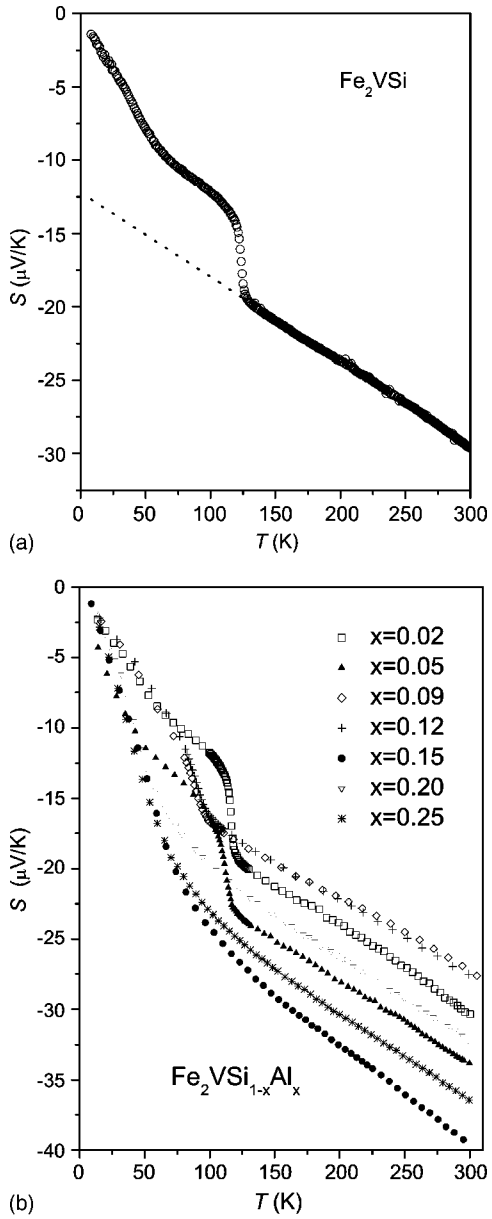

FIG. 4. (a) Seebeck coefficient vs temperature in Fe_2VSi. The dotted line is fit to the class formula for the diffusion thermopower. (b) Evolution of the temperature-dependent Seebeck coefficient in $Fe_2VSi_{1-x}Al_x$.

but become less visible for the highly substituted ones. The anomalous feature is much more apparent in a dS/dT vs T plot, as shown in Fig. 5. Since S is not influenced by intergrain transport, it should reflect more intrinsic properties of the studied materials. We thus determined the transition temperature T_s using the position of the negative dip in dS/dT for each composition. Clearly, T_s shifts to low temperatures with increasing Al content accompanied by a broadening of the transition interval. A weak but detectable dip near 40 K is still resolved in $Fe_2VSi_{0.80}Al_{0.20}$ (see the inset of Fig. 5), suggesting that the cubic $L2_1$ phase is not yet completely stable in this composition. The broader transition width for the higher Al concentration is attributed to disorder, consistent with ρ and κ results. It is noted that $Fe_2VSi_{0.98}Al_{0.02}$

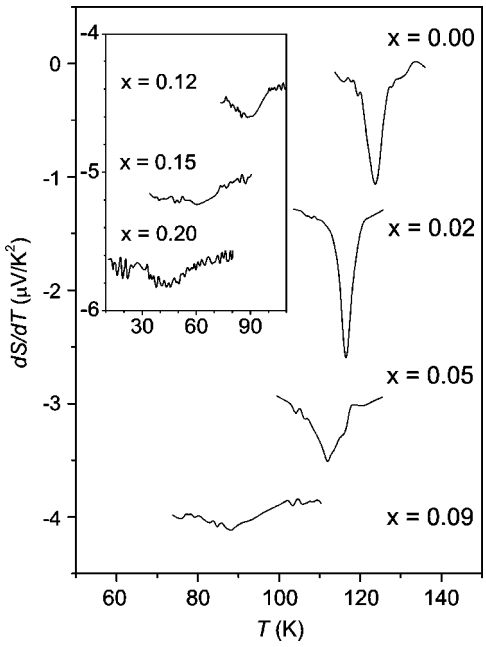

FIG. 5. Temperature dependence of dS/dT in $Fe_2VSi_{1-x}Al_x$ near T_s. Each curve is offset for clarity.

seems to have less disorder than that of the stoichiometric Fe_2VSi, as evidenced by the narrower transition width in dS/dT. In spite of this fact, the transition temperature in Fe_2VSi is still higher than that of $Fe_2VSi_{0.98}Al_{0.02}$, indicating that disorder has little effect on the variation of structural transition in these low-substituted $Fe_2VSi_{1-x}Al_x$ alloys.

E. Heat capacity

Heat capacity measurement is known as a sensitive probe of phase transitions involving entropy change. The measured heat capacity of $Fe_2VSi_{1-x}Al_x$ are plotted in Fig. 6. For clarity, each curve is offset by 25 J/mol K starting form $x=0.25$. In the inset of Fig. 6, a hysteresis loop of about 4 K for $Fe_2VSi_{0.98}Al_{0.02}$ is displayed, consistent with the ρ result. Such thermal hysteretic behavior actually for all $Fe_2VSi_{1-x}Al_x$ alloys with transition (not shown here), confirming that the presented phase transitions are first-order in nature.

Distinct peaks in C_P are clearly seen near the corresponding transition temperatures. The heat capacity jump ΔC_P near the transitions can be estimated by subtracting the smooth lattice background of the $x=0.25$ sample. As demonstrated, the height of ΔC_P progressively reduces with increasing the substitution level. Also the entropy change (ΔS) associated with the structural transition can be obtained by integrating the corresponding $\Delta C_P/T$ with temperature. The determined values in units of R (ideal gas constant) are tabulated in Table I. For the high Al content samples, heat capacity exhibits a monotonically Debye-like variation with no anomaly present over the temperature range we investigated. We connected these results to the disorder effect which broadens the transition width and thus smears out the transition peak as observed.

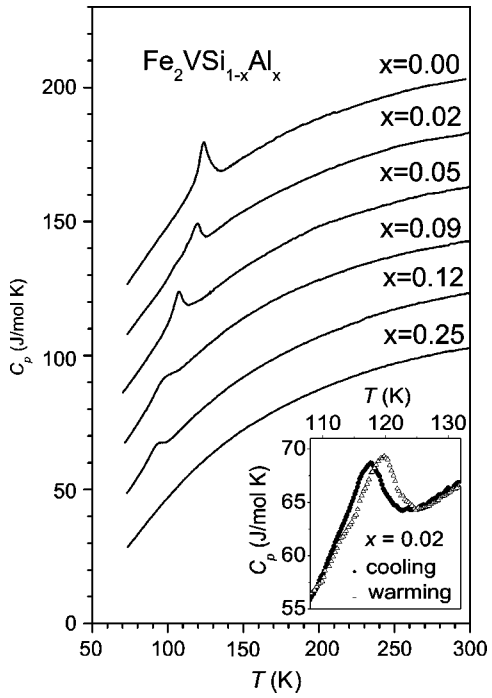

FIG. 6. Temperature variation of the observed heat capacity in $Fe_2VSi_{1-x}Al_x$. Each curve is offset by 25 J/mol K for clarity. The inset illustrates an enlarged view of the thermal hysteresis behavior for $Fe_2VSi_{0.98}Al_{0.02}$.

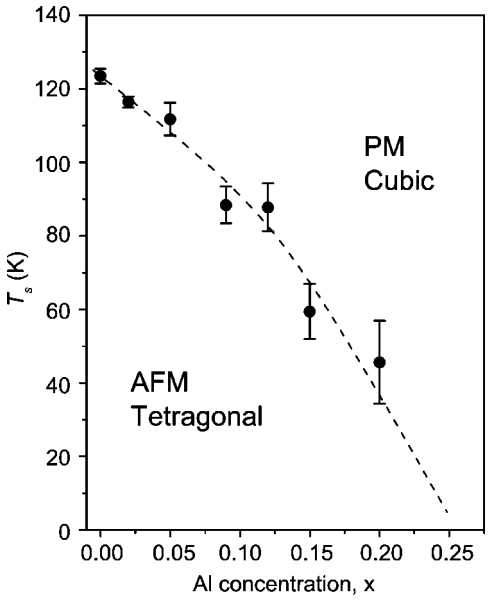

FIG. 7. Phase diagram in $Fe_2VSi_{1-x}Al_x$. Open circles correspond to the minimum temperature of dS/dT. The error bar is taken as the full width at half maximum (FWHM) of dS/dT around the transition. The dashed curve is guided to the eye for the phase boundary.

F. Phase diagram and calculated density of states of $Fe_2VSi_{1-x}Al_x$

According to the above results, the phase diagram between temperature and Al concentration of $Fe_2VSi_{1-x}Al_x$ can be concluded as given in Fig. 7. The phase boundary between the high-T paramagnetic cubic structure and low-T antiferromagnetic tetragonal structure is thus established. It shows that doping with Al in Fe_2VSi gradually reduces the transition temperature and consequently leads to the disappearance of transition at $x \approx 0.25$. On the contrary, the reported phase diagrams for $Fe_2V_{1-x}Cr_xSi$ and $Fe_2V_{1-x}Mn_xSi$ exhibit rather different tendency.[34] The Cr- and Mn-substituted systems show that T_s decreases more rapidly with the substitution level x and vanishes at $x \approx 0.08$. In fact, the replacement of V with Cr and Mn results in the change of hybridization between d bands, while substitution on the sites of nonmagnetic ligand atoms simply varies the conduction electron density. Therefore, as compared with these cases, we believe that both mechanisms play different roles for stabilizing the high-T $L2_1$ structure of Fe_2VSi.

From the recent band structure calculations on Fe_2VSi,[33] we notice that Fe has a peak near the Fermi level density of states (DOS) which splits from the cubic structure to the tetragonal one. Such behavior is quite similar to that found in the Heusler alloy, Ni_2MnGa,[41] in which Ni has a peak near the Fermi level and the peak in the cubic phase splits as transforming to the tetragonal structure. Other isostructural systems, e.g., Co_2NbSn and Ni_2FeGa,[41–43] also exhibit similar tendency from the high-temperature $L2_1$ phase to the low-temperature orthorhombic structure. The splitting behavior, arising from the reduction of symmetry, has been proposed to be driven by a band Jahn-Teller distortion.[41] Therefore, it was considered that the splitting of Fe partial DOS is a significant ingredient for the observed structural transition in Fe_2VSi.

In order to further address this scenario, we performed *ab initio* calculations to obtain the DOS for both AFM and PM cases with the substituted level $x=0$, 0.0625, 0.125, 0.25, and 0.5. The presented DOSs were obtained by a minimization of the total energy with respect to the volume. Total energy of the systems were determined in the framework of spin-polarized density functional theory.[44] The proposed generalized gradient approximation (GGA) by Perdew and Wang[45] was used for the nonlocal correction to a purely local treatment of the exchange-correlation potential and energy. The single-particle Kohn-Sham equations[46] were solved using the plane-wave-based Vienna *ab initio* simulation program (VASP) developed at the Institut für Material Physik of the Universität Wien.[47] The interactions between the ions and valence electrons are described by the projector augmented-wave (PAW) method[48] in the implementation of Kresse and

TABLE II. The changes in total energy of the paramagnetic cubic phase and the antiferromagnetic tetragonal phase in unit of electron-volts for the cells containing 8 Fe atoms.

% of Al	0	6.25	12.5	25
E_{cub}-E_{tetra}	0.32	0.27	0.22	0.14

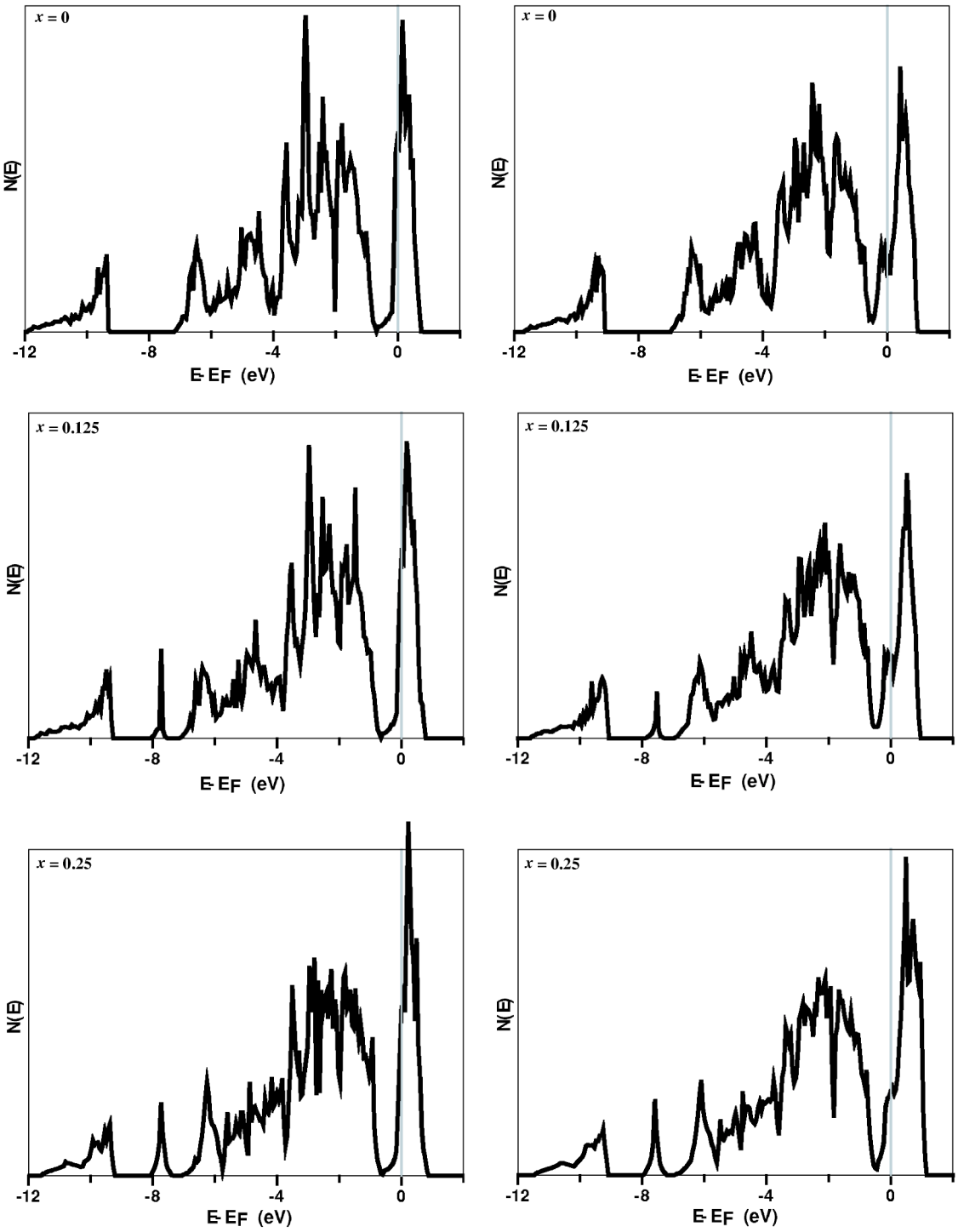

FIG. 8. Total density of states for paramagnetic (left panels) and antiferromagnetic phases (right panels) of $Fe_2VSi_{1-x}Al_x$. The Fermi level is indicated by a vertical broken line.

Joubert.[49] The numbers of treated valence electrons are 8, 5, 4, and 3 for Fe, V, Si, and Al atoms, respectively. The energy cutoff for the plane-wave basis is 270 eV in all calculations. The Monkhorst-Pack[50] method of sampling k points is used for the Brillouin-zone integration.

The calculated lattice constants (a) for the cubic Fe_2VSi is 0.561 nm and that for the tetragonal phase is 0.568 nm with 0.97 for the value of c/a ratio; the experimental values[34] of the tetragonal phase are 0.5685 nm for a and 0.988 for c/a ratio. The Monkhost-Pack parameters (9 9 9) were used for the unit cells which consist of 8 Fe atoms 4 V atoms and 4 Si atoms while (13 13 13) were used in calculating the density of states. The same density in k-point sets was used in the calculations of larger unit cells with Al doping. The calculated local moment for Fe in the tetragonal Fe_2VSi was found to be $0.784\mu_B$.

All doping systems are simulated by supercells and the percent of Al doping investigated in the present study includes 6.25, 12.5, 25, and 50, i.e., the largest cell used is $Fe_{32}V_{16}Si_{15}Al$. Relaxation processes for atoms were accomplished by moving atoms to the positions at which all atomic forces are smaller than 0.2 eV/nm and the cell dimensions were also allowed to relax. The calculated energy differences are listed in Table II. In the case of 50% doping, i.e., $Fe_2VSi_{0.5}Al_{0.5}$, the initial tetragonal phase was found to become almost cubic after relaxation with tiny energy difference from the cubic phase. The phase transition is thus expected to be completed by 50% doping.

In Fig. 8, we presented the calculated DOS for the $Fe_2VSi_{1-x}Al_x$ system with $x=0$, 0.125, and 0.25. The results of the paramagnetic and antiferromagnetic phases are illustrated in the left and right panels of Fig. 8, respectively. It is found that the DOSs are very similar for the cubic structure while the benefit of a split shoulder near the Fermi energy for the preference of the tetragonal phase is gradually lost as the percent of Al doping is increased. Our calculations are thus consistent with experimental observations, demonstrating that the $L2_1$ cubic structure is stabilized with substituted level $x \geqslant 0.25$ in $Fe_2VSi_{1-x}Al_x$. It also implies that the splitting of Fe partial DOS, presumably due to a band Jahn-Teller distortion, plays an important role for the structural stabilization in Fe_2VSi.

IV. CONCLUSIONS

In summary, structural, thermal, as well as transport properties in the Heusler-type compounds $Fe_2VSi_{1-x}Al_x$ were studied. Pronounced anomalies associated with structural phase transition were observed with $x<0.25$. Experimental data can be interpreted coherently with those obtained from *ab initio* calculations. Both yield a possible disappearance of the structural transition beyond a critical concentration $x_C \approx 0.25$, indicating that the replacement of Si with Al stabilizes the cubic phase of Fe_2VSi. The conclusions made in this study provide a significant understanding to the structural phase transition in Fe_2VSi, and should be relevant to other Heusler compounds that undergo a cubic $L2_1$ to a tetragonal or orthorhombic structure transition.

ACKNOWLEDGMENTS

This work was supported by the National Science Council of Taiwan under Grant Nos. NSC-93-2112-M-006-001 (C.S.L.) and NSC-93-2112-M-259-004 (Y.K.K.). The computer resources were partly provided by the the National Center for High-Performance Computing in HsinChu, Taiwan.

*Electronic address: ykkuo@mail.ndhu.edu.tw

[1] K. H. J. Buschow and P. G. van Engen, J. Magn. Magn. Mater. **25**, 90 (1981).
[2] C. S. Lue and Y.-K. Kuo, Phys. Rev. B **66**, 085121 (2002).
[3] K. Kobayashi, R. Y. Umetsu, R. Kainuma, K. Ishida, T. Oyamada, A. Fujita, and K. Fukamichi, Appl. Phys. Lett. **85**, 4684 (2004).
[4] A. Slebarski, J. Deniszczyk, W. Borgie, A. Jezierski, M. Swatek, A. Winiarska, M. B. Maple, and W. M. Yuhasz, Phys. Rev. B **69**, 155118 (2004).
[5] M. Weinert and R. E. Watson, Phys. Rev. B **58**, 9732 (1998).
[6] A. Bansil, S. Kaprzyk, P. E. Mijnarends, and J. Tobola, Phys. Rev. B **60**, 13 396 (1999).
[7] I. Galanakis, P. H. Dederichs, and N. Papanikolaou, Phys. Rev. B **66**, 174429 (2002).
[8] A. Kellou, N. E. Fenineche, T. Grosdidier, H. Aourag, and C. Coddet, J. Appl. Phys. **94**, 3292 (2003).
[9] P. J. Webster, K. R. A. Zeibeck, S. L. Town, and M. S. Peak, Philos. Mag. B **49**, 295 (1984).
[10] M. Terada, Y. Fujita, and K. Endo, J. Phys. Soc. Jpn. **36**, 620 (1974).
[11] M. Wuttig, J. Li, and C. Craciunescu, Scr. Mater. **44**, 2393 (2001).
[12] Z. H. Liu, M. Zhang, Y. T. Cui, Y. Q. Zhou, W. H. Wang, G. H. Wu, X. X. Zhang, and G. Xiao, Appl. Phys. Lett. **82**, 424 (2003).
[13] K. Ullakko, J. K. Huang, C. Kanter, R. C. O'Handley, and V. V. Kokorin, Appl. Phys. Lett. **69**, 1966 (1996).
[14] R. Tickle and R. D. James, J. Magn. Magn. Mater. **195**, 627 (1999).
[15] R. C. O'Handley, S. J. Murray, M. Marioni, H. Nembach, and S. M. Allen, J. Appl. Phys. **87**, 4712 (2000).
[16] A. Sozinov, A. A. Likhachev, N. Lanska, and K. Ullakko, Appl. Phys. Lett. **80**, 1746 (2002).
[17] V. K. Pecharsky and K. A. Gschneidner, Jr., Phys. Rev. Lett. **78**, 4494 (1997).
[18] A. Ayuela, J. Enkovaara, K. Ullakko, and R. M. Nieminen, J. Phys.: Condens. Matter **11**, 2017 (1999).
[19] K. U. Neumann, T. Kanomata, B. Ouladdiaf, and K. R. A. Ziebeck, J. Phys.: Condens. Matter **14**, 1371 (2002).
[20] C. S. Garde and J. Ray, J. Phys.: Condens. Matter **14**, 3775 (2002).
[21] F. Casanova, A. Labarta, X. Batlle, J. Marcos, L. Manosa, A. Planes, and S. de Brion, Phys. Rev. B **69**, 104416 (2004).
[22] E. M. Levin, K. A. Gschneidner, Jr., T. A. Lograsso, D. L. Schlagel, and V. K. Pecharsky, Phys. Rev. B **69**, 144428 (2004).
[23] K. Endo, H. Matsuda, K. Ooiwa, and K. Itoh, J. Phys. Soc. Jpn. **64**, 2329 (1995).
[24] M. Kawakami, S. Nishizaki, and T. Fujita, J. Phys. Soc. Jpn. **64**, 4081 (1995).
[25] M. Kawakami, K. Yamaguchi, and T. Shinohara, J. Phys. Soc. Jpn. **68**, 2128 (1999).
[26] V. Niculescu, T. J. Burch, K. Raj, and J. I. Budnick, J. Magn. Magn. Mater. **5**, 60 (1977).
[27] H. Nishihara, K. Ono, K. U. Neumann, K. R. A. Ziebeck, and T. Kanomata, Physica B **329–333**, 1107 (2003).
[28] S. Jemima, A. Mani, A. Bharathi, N. Ravindran, and Y. Hariharan, J. Alloys Compd. **326**, 183 (2001).
[29] O. Nashima, T. Kanomata, Y. Yamaguchi, S. Abe, T. Harada, T.

Suzuki, H. Nishihara, K. Koyama, T. Shishido, K. Watanabe, and T. Kaneko, J. Alloys Compd. **383**, 298 (2004).
[30] C. S. Lue and J. H. Ross, Jr., Phys. Rev. B **61**, 9863 (2000); **63**, 054420 (2001).
[31] A. U. B. Wolter, A. Bosse, D. Baabe, I. Maksimov, D. Mienert, H. H. Klaus, F. J. Litterst, D. Niemeier, R. Michalak, C. Geibel, R. Feyerherm, R. Hendrikx, J. A. Mydosh, and S. Sullow, Phys. Rev. B **66**, 174428 (2002).
[32] Y.-K. Kuo, C. S. Lue, F. H. Hsu, H. H. Li, and H. D. Yang, Phys. Rev. B **64**, 125124 (2001).
[33] S. Fujii, S. Ishida, and S. Asano, J. Phys. Soc. Jpn. **73**, 459 (2004).
[34] M. Kawakami and T. Uchimura, J. Phys. Soc. Jpn. **67**, 2758 (1998).
[35] C. M. Hurd, I. Shiozaki, and S. P. McAlister, Phys. Rev. B **26**, 701 (1982).
[36] Y. K. Kuo, K. M. Sivakumar, W. J. Lai, and C. S. Lue (unpublished).
[37] J. F. Wan, X. L. Lei, S. P. Chen, and T. Y. Hsu, Phys. Rev. B **70**, 014303 (2004).
[38] C. S. Lue, Y.-K. Kuo, C. L. Huang, and W. J. Lai, Phys. Rev. B **69**, 125111 (2004).
[39] M. Ziman, *Electrons and Phonons* (Oxford University Press, London, 1960).
[40] J. Sakurai, Y. Yamamoto, and Y. Komura, J. Phys. Soc. Jpn. **57**, 24 (1988).
[41] S. Fujii, S. Ishida, and S. Asano, J. Phys. Soc. Jpn. **58**, 3657 (1989).
[42] A. Yamasaki, S. Imada, R. Arai, H. Utsunomiya, S. Suga, T. Muro, Y. Saitoh, T. Kanomata, and S. Ishida, Phys. Rev. B **65**, 104410 (2002).
[43] Z. H. Liu, H. N. Hu, G. D. Liu, Y. T. Cui, M. Zhang, J. L. Chen, G. H. Wu, and G. Xiao, Phys. Rev. B **69**, 134415 (2004).
[44] P. Hohenberg and W. Kohn, Phys. Rev. **136**, B864 (1964).
[45] J. P. Perdew, in *Electronic Structure of Solids '91*, edited by P. Ziesche and H. Eschrig (Akademie-Verlag, Berlin, 1991); J. P. Perdew, J. A. Chevary, S. H. Vosko, K. A. Jackson, M. R. Pederson, D. J. Singh, and C. Fiolhais, Phys. Rev. B **46**, 6671 (1992).
[46] W. Kohn and L. J. Sham, Phys. Rev. **140**, A1133 (1965).
[47] G. Kresse and J. Hafner, Phys. Rev. B **47**, R558 (1993); **49**, 14251 (1994); G. Kresse and J. Furthmüller; *ibid.* **54**, 11169 (1996); G. Kresse and J. Furthmüller, Comput. Mater. Sci. **6**, 15 (1996).
[48] P. E. Blöchl, Phys. Rev. B **50**, 17 953 (1994).
[49] G. Kresse and D. Joubert, Phys. Rev. B **59**, 1758 (1999).
[50] H. J. Monkhorst and J. D. Pack, Phys. Rev. B **13**, 5188 (1976).